phys. stat. sol. (a) **187**, No. 1, 257–274 (2001)

Models in Heterogeneous Catalysis: Surface Science Quo Vadis?

H.-J. FREUND[1]), N. ERNST, T. RISSE, H. HAMANN, and G. RUPPRECHTER

Fritz-Haber-Institut der Max-Planck-Gesellschaft, Department of Chemical Physics Faradayweg 4-6, D-14195 Berlin, Germany

(Received March 9, 2001; accepted July 12, 2001)

Subject classification: 68.35.Dv; 68.35.Fx; 68.35.Md; 68.35.Np; 68.37.Ef; 68.37.Lp; 68.43.Pq; 68.47.Gh; 68.47.Jn; 68.55.Ac; 75.50.Tt; 75.70.Rf; 78.60.Hk

Model catalyst systems have been prepared by growth of small metal aggregates on thin well ordered oxide films of alumina and silica. These systems lend themselves to structural and morphological characterization via scanning probe microscopies and transmission electron microscopy and bridge to a certain extent the materials gap between metal single crystal studies and the investigation of real catalyst samples. Recently, the classical surface science techniques applied under ultrahigh vacuum conditions have been augmented by non-linear optical techniques, such as sum frequency generation, which can also be applied under ambient gas pressures. Thus, the pressure gap between studies in surface science under realistic conditions can be bridged.

1. Introduction

Surface science and catalysis have a lot in common but they are still separated by materials as well as pressure gaps. To bridge these gaps is a task that has to be taken up and surface science has reached a degree of maturity that should allow us to achieve this goal. The use of model systems is one strategy for bridging the gaps [1, 2]. A wide variety of systems serve as models of practical catalysts. Briefly, the various approaches share the requirement that the substrate onto which the model is built should be electrically conducting, to allow application of the appropriate surface science tools, as shown in Fig. 1 [3–7]. The catalyst support is prepared on these substrates as a thin layer, because most practical supports, such as magnesia, alumina, or silica, are insulators. When they are thin, these layers are sufficiently conductive to allow application of analytical methods based on sample interrogation with charged particles without severe charging of the sample.

In this paper we discuss structure and properties of metal aggregates prepared by evaporation, nucleation and growth on thin, well-ordered oxide films. It is obvious that the advent of STM has had a substantial influence on our understanding of morphology in growth processes and the STM is particularly well suited for systems based on thin oxide films. Goodman's group, Somorjai's group as well as our own group have made contributions to this field.

2. Preparation, Growth and Morphology

In the preceding few years, several strategies have been followed to prepare and study model catalyst systems [8]. In early work, small metal particles were deposited onto oxide

[1]) Tel.: +49-30-8413-4100; FAX: +49-30-8413-4101; e-mail: freund@fhi-berlin.mpg.de

 0031-8965/01/18709-0257 $ 17.50+.50/0

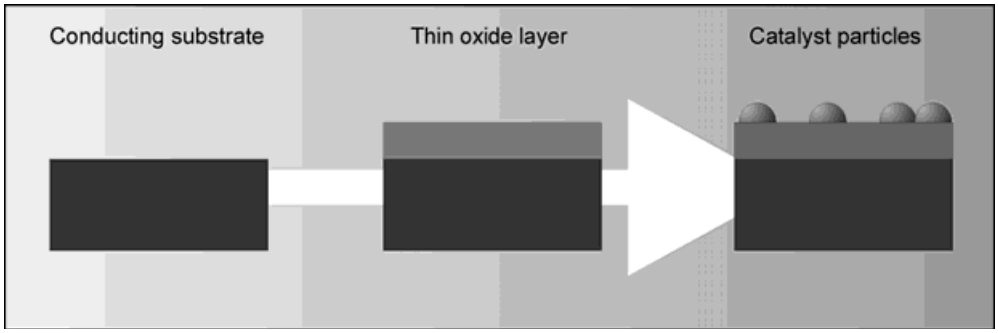

Fig. 1. Schematic diagram of model catalyst systems

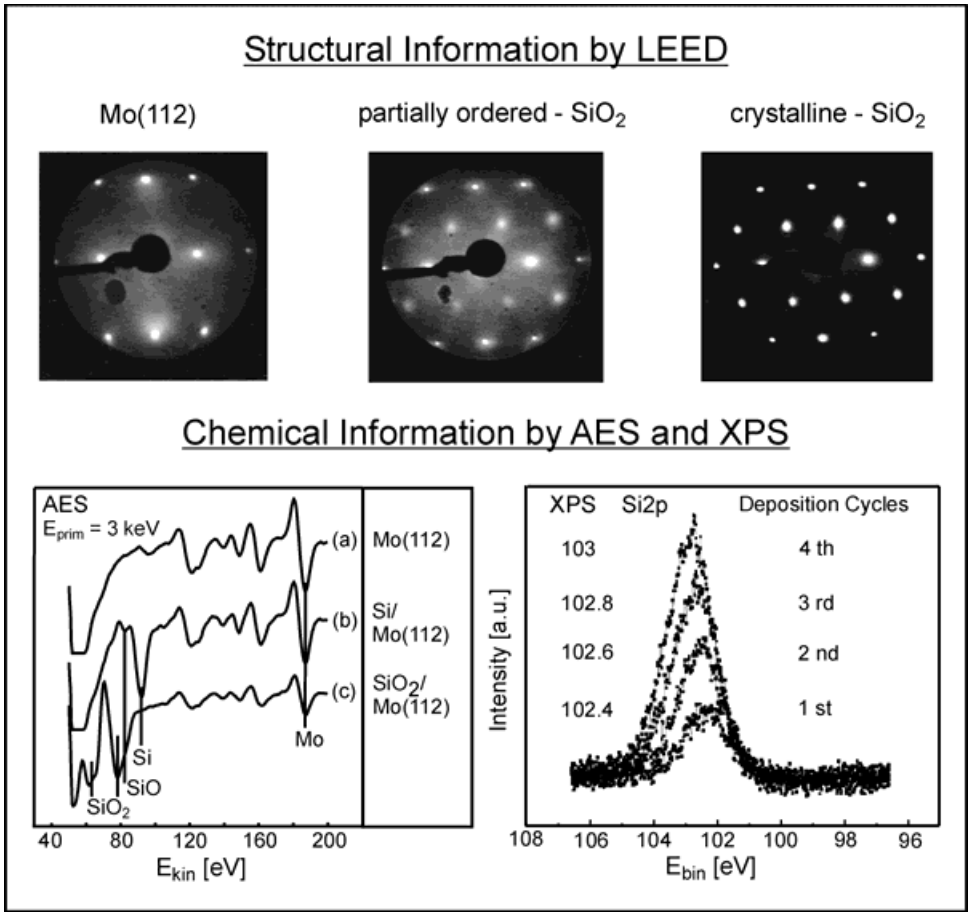

Fig. 2. Above: LEED pattern of the commensurate silica epilayer on Mo(112);
Lower part: Si LVV Auger transition (left) and Si 2p XP spectra (right) prove the stoichiometry of the SiO_2 layer on M(112)

bulk single-crystal surfaces, particularly MgO, and characterized by transmission electron microscopy (TEM). Poppa [9] was the pioneer in this field; important contributions have been reviewed recently by Henry, who was involved in the early TEM measurements [10].

The early efforts were primarily aimed at the preparation of small, well-defined metal particles; another strategy has been followed by Møller et al. [11–14] and Diebold et al. [15], who prepared thin metal layers on bulk oxide single crystals, such as TiO_2(110). As mentioned above, the advent of scanning tunneling microscopy has had a substantial influence on the understanding of the structures of clean oxide surfaces. Several groups [16-18] have begun investigating metal deposition on TiO_2 surfaces. Interesting initial results have been obtained concerning metal particle migration and oxide migration onto the metal particles (the so-called SMSI effect) [17, 18].

Recently, it has been shown that ordered thin silica layers can be grown [19]. In our laboratory, a silica layer has been prepared on Mo(112). Fig. 2 shows a LEED pattern of the layer prepared by evaporation of silicon and subsequent oxidation. The surface has hexagonal symmetry, but its detailed structure is not yet known. Included in Fig. 2 is a set of Si2p photoelectron spectra shown as a function of layer thickness and preparation conditions. The value observed for the final preparation is practically identical to that observed for thin silica layers on silicon, which are generally known to be amorphous [20]. These layers will be used in the future as supports for evaporated metal aggregates.

In the past we have used primarily well-ordered alumina layers as substrates; in Fig. 3 we show the result of an STM investigation. The left panel shows the clean alumina surface as imaged by a scanning tunneling microscope [21]. The surface is well ordered, and there are several kinds of surface defects. One constitutes reflection domain boundaries between the two growth directions of Al_2O_3(0001) on the NiAl(110) sur-

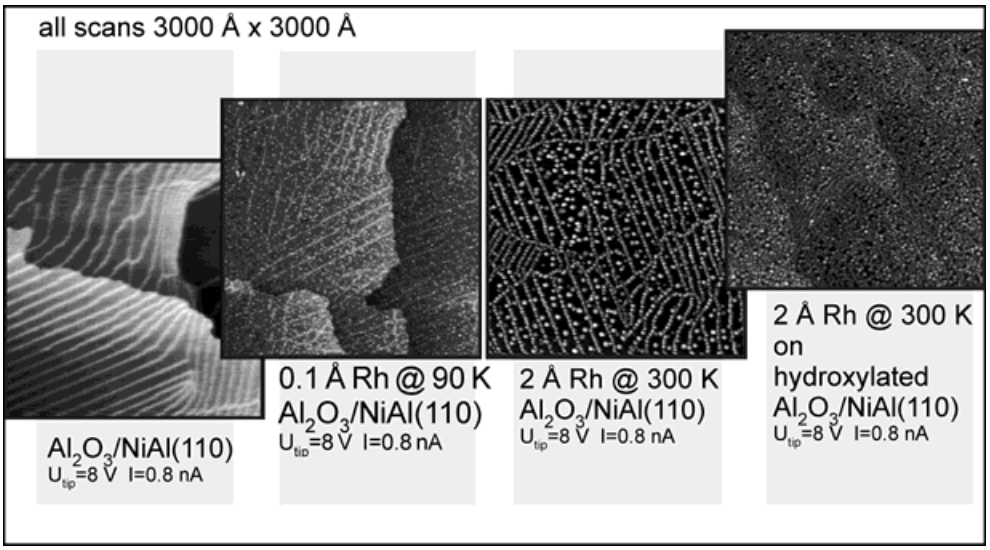

Fig. 3. Scanning tunneling microscopic images of a clean alumina layer (from left to right), after deposition of 0.1 Å of rhodium at 90 K, after deposition of 2 Å of rhodium at 300 K, and after deposition of 2 Å of rhodium at 300 K onto the prehydroxylated alumina layer. All scans: 3000 × 3000 $Å^2$

face, the substrate on which the layer was grown according to a well-established oxidation recipe [22]. There are anti-phase domain boundaries within the reflection domains, and, in addition, point defects which are not resolved in the images. The image does not change dramatically after hydroxylation of the layer [23]. The additional panels show STM images of rhodium deposits on the clean surface at low temperature and at room temperature [4, 24], as well as an image recorded after deposition of rhodium at room temperature on a hydroxylated substrate [25]. The amount deposited onto the hydroxylated surface is equivalent to the amount deposited onto the clean alumina surface at room temperature. Upon vapor deposition of rhodium at low temperature, small particles were observed to nucleate on the point defects of the substrate, yielding a narrow distribution of particle sizes. When the deposition of rhodium is carried out at room temperature, the mobility of rhodium atoms is considerably higher than that at low temperature, so that nucleation at the line defects of the substrate becomes dominant. Consequently, most of the material nucleates on reflection domain and anti-phase domain boundaries. The particles are relatively uniform in size, with the size depending on the amount of material deposited. When the same amount of material is deposited onto a hydroxylated surface, the particles are considerably smaller and distributed across the entire surface, i.e., a much higher metal dispersion is obtained [23].

The thermal behavior of the deposits is important to chemical reactivity, because the particles may undergo morphological changes to adopt their equilibrium shapes, which could depend on whether or not a reactive gas phase is present. In the present case, detailed experiments have been undertaken to characterize the particles deposited onto the clean substrate, and less detailed experiments have been done to characterize the deposits on the hydroxylated surface [4]. As a result of these investigations, it is known that the morphology of the ensemble is not altered within a temperature window from 90 to approximately 450–600 K. The window is extended to even higher temperatures when the substrate is hydroxylated. At temperatures above the upper limit, the particles tend to sinter, and they also start to diffuse through the layer into the metal substrate below [4].

While it is straightforward to image the morphology of the systems, it is more difficult to image the surface structure of these aggregates at atomic resolution. There are only a few reported investigations of deposited metal particles at atomic resolution. The first report of an atomically resolved image of a palladium metal cluster on MoS_2 was reported by Piednoir et al. [26]. Atomically resolved images of palladium aggregates deposited on a thin alumina layer have also been obtained [27]. Figure 4 shows such an image of an aggregate of about 80 Å in width. The particle is obviously crystalline and exposes on its top a (111) facet. Furthermore, on the side, (111) facets (typical of a cuboctahedral particle) can be discerned. The small (100) facets predicted for equilibrium shape considerations on the basis of the Wulff construction could not be atomically resolved. However, if we apply the concept of the Wulff construction, we may deduce the metal surface adhesion energy [27]. The basic equation is

$$W_{\mathrm{adh}} = \gamma_{\mathrm{oxide}} + \gamma_{\mathrm{metal}} - \gamma_{\mathrm{interface}} \,. \tag{1}$$

Provided the surface energies (γ_{metal}) of the various crystallographic planes of the metal are known [28], a relative work of adhesion (W_{adh}) may be defined [27]. We find a value of 2.9 ± 0.2 J/m^2, which is still rather different from the result of recent calculations by Jennison et al. [29], who reported metal adsorption energies of 1.05 J/m^2 calculated for a thin defect-free alumina layer. It is not unlikely that this discrepancy is

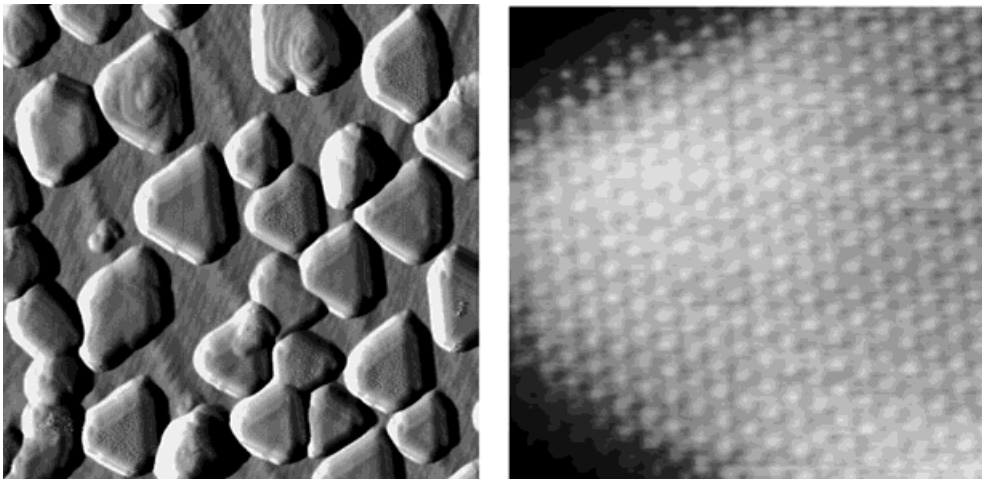

Fig. 4. Scanning tunneling images at atomic resolution of Pd aggregates grown on an alumina film (left 500 × 500 Å^2, right 50 × 50 Å^2) [27]

related to the rather complicated nucleation and growth behavior of the aggregates involving defects of the substrate.

Although STM reveals the surface structure of deposited particles, their internal structure, in particular as a function of size, is not easily accessible from STM images. In this connection, TEM images of the model systems can be of help [30]. TEM allows the determination of interatomic distances as a function of cluster size. For the case of Pt on the thin alumina film, this is shown in Fig. 5. The atomic distances decrease

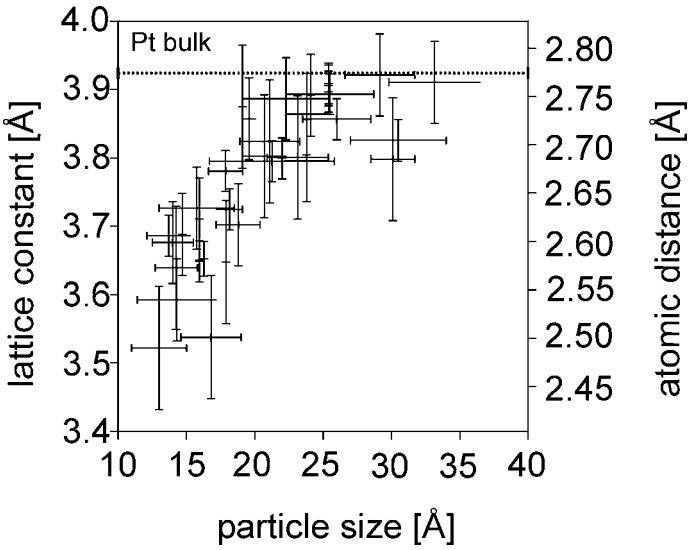

Fig. 5. Lattice constants and interatomic distance of platinum particles grown on Al_2O_3/NiAl(110) as a function of their size. (The ends of the horizontal bars represent the width and the length of the particular particles, respectively, and the vertical bars are error bars.)

continuously to 90% of the bulk value at a cluster size of 10 Å. On the other hand, the lattice constant approaches the platinum bulk value even at a diameter of 30 Å. This effect has been detected for tantalum and for palladium clusters on thin alumina layers too, but it seems to be less pronounced in these cases.

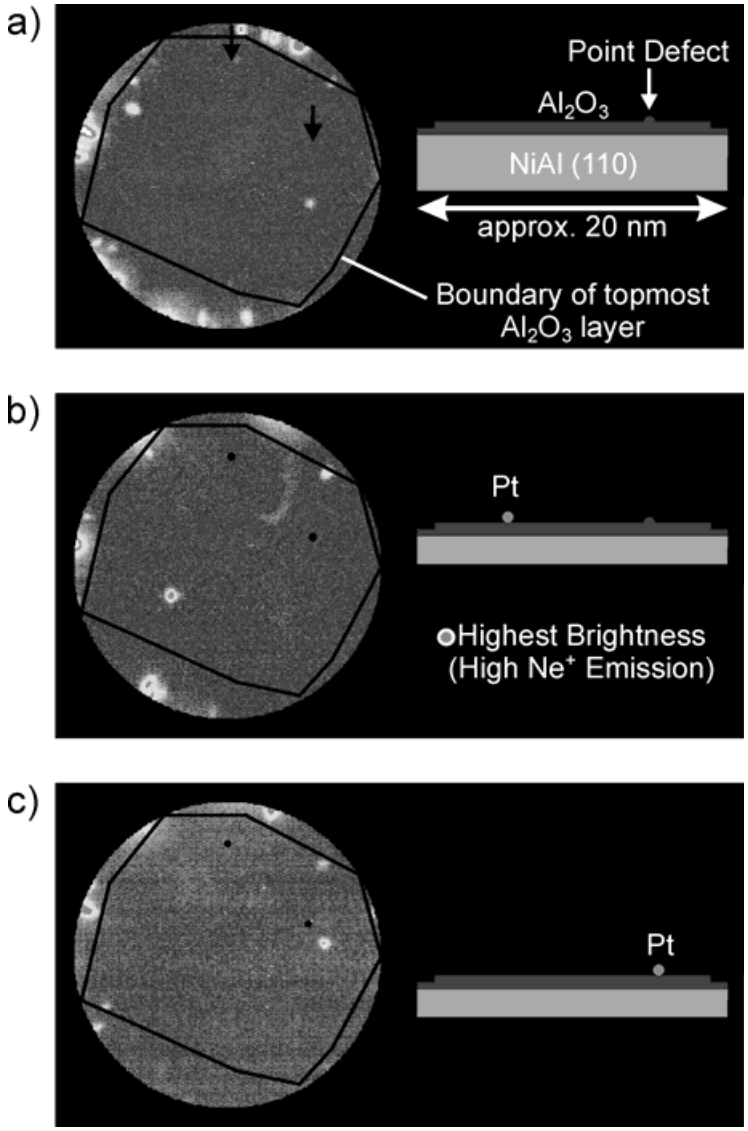

Fig. 6. Surface diffusion of Pt/AL_2O_3/NiAl(110). The polygon curves had been drawn in the circular sections of the FIM patrtern to indicate the boundary of the topmost Al_2O_3 layer: a) Before deposition; b) after deposition, an individual Pt adatom was imaged at 35 K using neon-FIM at 7.7 keV (black dots: positions of defects); c) aftger heatingh the surface to 170 K during 20 s at zero field

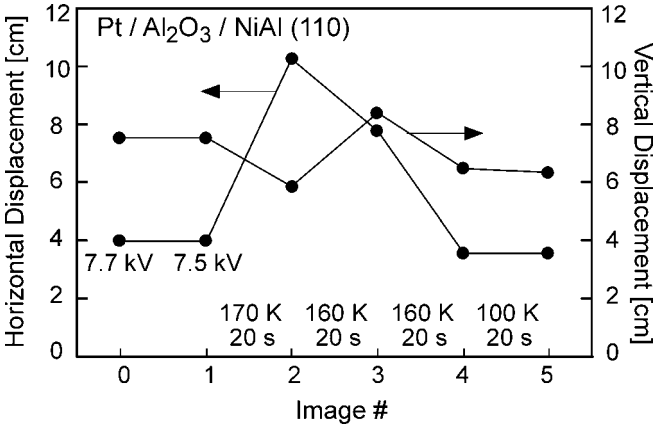

Fig. 7. Positions of image spots of Pt adatoms diffusing on AL_2O_3/NiAl(110). Between the imaging cycles the temperature was varied from 170 K (Fig. 6c) to 100 K

An interesting field of investigation is the study of processes that lead to cluster formation and to cluster growth. Diffusion of metal atoms on oxide surfaces is the inherent basic process. The obvious method to perform a study on diffusion is scanning tunneling microscopy. However, in contrast to diffusion studies on metal surfaces, similar studies on oxide surfaces have not been reported. On the other hand, field ion microscopy is being used in our group to study such processes. Applying neon-FIM at 79 K the feasibility to image platinum adatoms, supported on a thin alumina film grown on a [110]-oriented NiAl tip, had been demonstrated in our group [31]. At these conditions, the imaging of an *ensemble* of Pt adatoms is characterized by strong fluctuations and non-optimum contrast, partly compensated by computer aided image processing. Intending to observe cluster formation, the oxide surface had been exposed to a rela-

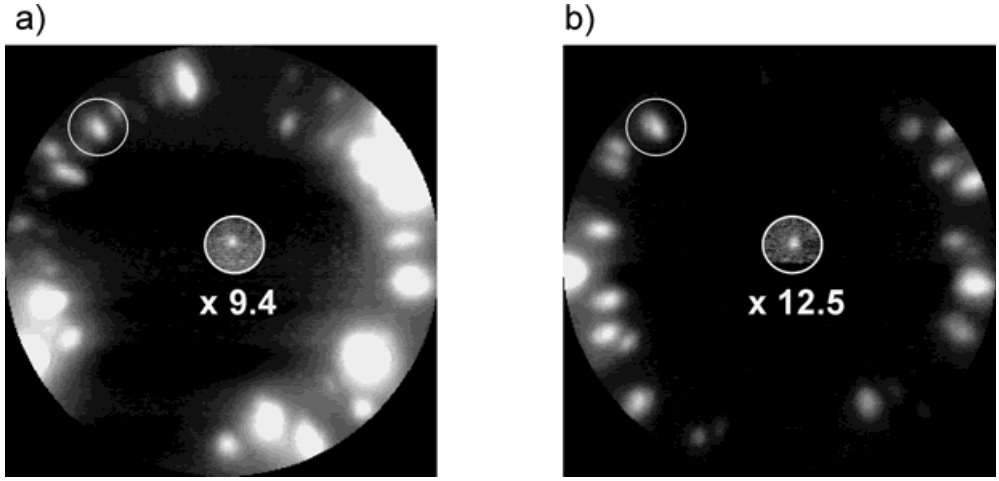

Fig. 8. Onset of surface diffusion of a Pt adatom adsorbed in the center of an alumina film on NiAl(110): To improve the visibility, the intensity around the image spot of the adatom was multiplied by a factor 9.4 (a) and 12.5 (b). Image b) was taken after 15 s heating at 100 K without applied field. The circle at "eleven o'clock" marks the position of a step site serving as a reference at the boundary

tive high platinum dose followed by several heating cycles. As a result, a local ordering of platinum adatoms was obtained in the vicinity of a point defect; the arrangement of adatoms was compatible with the surface unit cell [31]. From a displacement analysis of the platinum adatom ensemble only a rough estimation of the diffusion activation energy was obtained. Recently, we have prepared an *individual* Pt adatom on the apex plane of an oxidized [110]-oriented NiAl tip using neon-FIM at 35 K [32]. A sequence of FIM patterns obtained in a first, exploratory experiment is shown in Fig. 6. Circular sections of FIM images show the specimen surface after oxidation. Before deposition of platinum the Al_2O_3 film was imaged allowing to visualize sites at the boundary and point defects as in Fig. 6a. After exposing the surface (at 35 K) to a platinum beam, a new emission site appeared which was interpreted as the image spot of a single platinum adatom.

Figure 7 gives a survey of exploratory examinations of the surface diffusion behavior for alumina-supported, individual platinum adatoms, based on FIM patterns such as in Fig. 6b and c. At 160 K the Pt adatom is in fact more mobile on the well ordered oxide film than on NiAl(110) [32]. The onset temperature for surface diffusion was especially examined in another experiment (Fig. 8), allowing to estimate a value for the activation energy [33]. The identity of the adatom, prepared in the center of the plane was ascertained before and after the diffusion steps. In particular, upon the first heating step to 100 K for 15 s, the adatom changed its position slightly, but noticeably. In this case, our analysis of the jump direction is compatible with the model visualized in Fig. 9 [34].

In Table 1, we have compiled experimental and theoretical results of surface diffusion parameter for individual Pt adatoms. Those deposited on a thin alumina film sup-

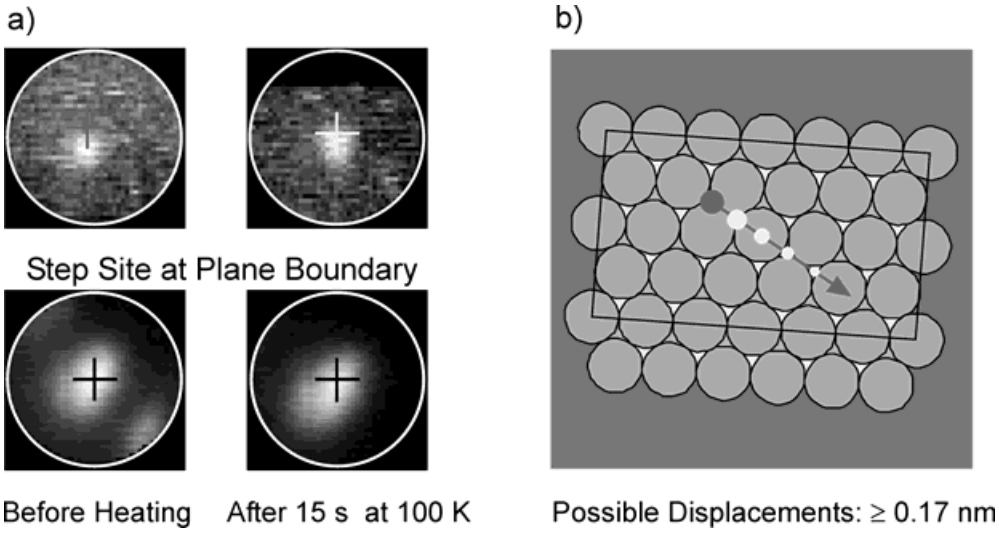

Fig. 9. Onset of surface diffusion. a) Experiment and b) model. The upper two enlarged FIM images in a) show positions of Pt adsorbed in the center of the alumina film prepared on NiAl(110) (Fig. 8). The lower two patterns display step sites whose image positions do not change upon heating. The model b shows a simplified, hexagonal arrangement of the top layer of oxygen ions and the surface unit cell. The thick, dark grey dot marks the position of the Pt adatom prior to heating. The smaller light dots show possible positions after the diffusion event. The maximum displacement is estimated to approximately 0.5 nm indicated by the decreasing diameter of light dots

Table 1
Surface diffusion parameter for individual Pt adatoms [32].

system	onset temperature (K)	activation energy (eV)
Pt/NiAl(110)	165	0.48
Pt/Ni(111)		<0.22 [33]
$Pt/Al_2O_3/NiAl(110)$	>100	>0.29
	<160	<0.47
$Pt/Al_2O_3/Al(111)$		0.7 [29]

ported on NiAl(110) showed an onset temperature for approaching 100 K. We note that our experimental estimate is probably close to 0.3 eV and thus significantly smaller than the calculated value, 0.7 eV obtained for $Pt/Al_2O_3/Al(111)$ [29]. Though further experiments are still required, we conclude that the activation energy of Pt on a defect free surface area of Al_2O_3 is comparable with results of Pt surface diffusion on closely packed metal surfaces such as Ni(111) and Pt(111) [33]. The relatively high mobility at temperatures approaching 100 K is also in general agreement with previous STM investigations on Pt cluster formation occurring at low temperatures on alumina [4]. It is clear, however, that the characterization of the surface diffusion behavior of alumina-supported platinum requires more displacement observations.

3. Electronic Structure of Individual Aggregates

Parallel to studying morphology, structure and processes of cluster formation, we have investigated the electronic structure of deposited metal aggregates. In earlier studies we have used photoelectron spectroscopy and X-ray absorption to investigate deposits with finite but narrow size distributions to probe the size dependent electronic structure of these systems [35]. With the advent of scanning tunneling microscopy it has become possible to investigate individual objects, and therefore the spectroscopy of optical and electronic properties of single, selected objects on a surface has been in the focus of interest in recent years. It opens the unique possibility to detect local variations in the electronic structure which are normally hidden in the inhomogeneous broadening of the spectra due to statistical disorder on the surface. A local measurement allows the direct connection between a distinct geometric structure and its optical, electronic or chemical properties. In this way, the opening of a size dependent band gap has been observed in small Pt clusters with scanning tunneling spectroscopy [36]. The catalytic activity of small Au clusters has been correlated with the appearance of the metal non-metal transition as cluster sizes decrease [37]. Spectroscopy of single molecules in the STM has demonstrated the great potential of investigating molecular vibrations as a function of adsorption site [38]. With the first observation of light emission from the tunnel junction of a STM, the detection of optical properties of a surface with nanometer resolution has become feasible [39]. The method has been employed to measure photon maps of metal and semiconductor surfaces, nanocrystals and individual molecules [40]. The spectroscopy of emitted photons provides an insight in the underlying elementary processes, whereby tip-induced plasmon resonances have been identified as the source of the observed photon emission [40]. These special interfacial modes are connected with the strong electromagnetic interaction between the tip and the sample in a STM and

are not visible in conventional optical spectroscopy. On the other side, typical features accessible to classical absorption spectroscopy, like Mie resonances in small metal particles or electronic transitions in molecules, have not been observed in the photon emission spectra from a tunnel junction of a STM. Therefore, there is still a gap to be bridged between conventional optical spectroscopy averaging over a macroscopic area of the surface and the emission spectroscopy in the STM at high spatial resolution. Here we report on photon emission from individual, alumina-supported Ag clusters [41]. The emission can clearly be distinguished from tip-induced plasmon modes and is interpreted as a decay of Mie-plasmon excitations in small metal particles, well known from absorption spectroscopy [42]. We have determined the Mie-plasmon energy and its homogeneous line width for single Ag particles as a function of cluster diameter between 1.5 and 12 nm.

In the experiment the tunnel tip of a beetle type STM, mounted in an UHV chamber, has been used as a local electron emitter. The electron energy could be adjusted in a wide range between 1–100 eV, the typical electron current was set to 1–10 nA. The electron injection from the tip caused electronic excitations in the sample followed by optical de-excitation processes. The emitted photons have been collected by a parabolic mirror surrounding the STM. Outside the vacuum chamber the light was focused onto the entrance slit of a grating spectrograph and detected with a liquid-nitrogen cooled CCD-camera. The spatial resolution of the emission spectroscopy depends on the tip–sample separation and therefore on the bias voltage applied. For tunnel voltages below 15 V the exciting electron current is restricted to an area smaller than 1.5 nm in diameter. Ag clusters were grown by vapor deposition at 300 K onto a thin, well-ordered alumina film prepared on a NiAl(110) single crystal [4]. The density of nucleation centers for the particles was controlled in a sputter-assisted deposition process. Depending on the amount of evaporated material the mean cluster size could be adjusted between 1 and 12 nm. The cluster diameter was determined after separating the effect of tip convolution. This was achieved by extracting a mean tip radius from the apparent broadening of step edges of the substrate.

The photon emission characteristics of a cluster-covered alumina film on NiAl(110) can be divided in two different excitation regimes depending on the tip voltage:

1. Spectra measured at low tunnel voltages (U_{tip} = 5 V) are dominated by two emission peaks at 1.3 eV and 2.4 eV, which are almost independent of polarity (Fig. 10, curve (i)). The emission is caused by collective electron oscillations in the coupled electron gases of tip and sample induced by a strong dynamic electromagnetic field in the tunnel cavity. Inelastically tunneling electrons are the driving force for these tip-induced plasmons [40]. The shape of the spectra is mainly determined by the dielectric function of NiAl. It can be reproduced within a theoretical model, which allows to calculate the electromagnetic response function of a simplified tip–sample geometry, using the dielectric function of the tungsten tip and the NiAl sample as material properties [43]. The thin alumina film and the presence of small metal clusters below the tunnel tip slightly modify the shape and intensity of the spectra emitted from the clean NiAl/W tunnel junction.

2. An increasing tunnel bias gradually decreases the tip–sample interaction and consequently the photon yield due to inelastic tunneling processes. At voltages above 10 V the characteristic lines of the tip-induced plasmon vanish. In contrast to the clean alumina surface, a new, intense emission line appears in the spectra taken on top of an Ag

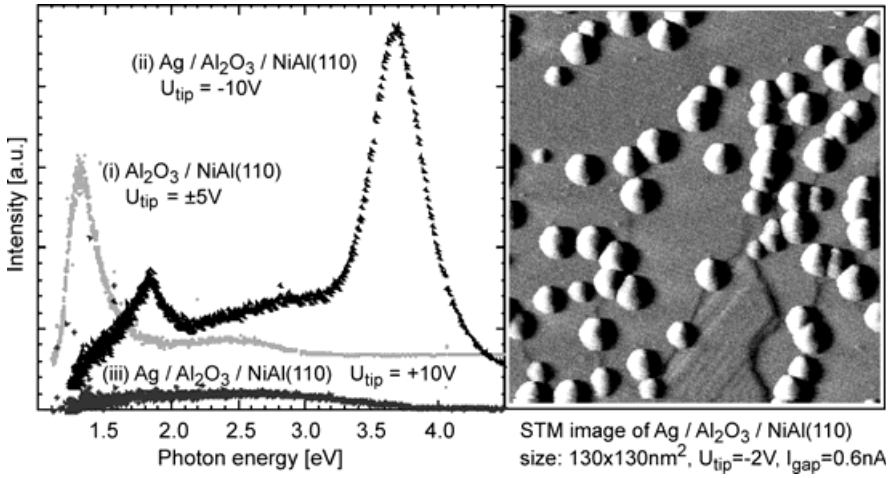

Fig. 10. Photon emission spectra at different tip voltages and STM image of $Ag/Al_2O_3/NiAl(110)$

cluster (Fig. 10, curve (ii)). The peak is centered around 3.7 eV and visible only for the injection of electrons from the tip into the cluster (see curve (iii) for comparison). The energetic position of the emission line corresponds to the (1,0)-mode of the Mie plasmon, well known from extinction cross section measurements on Ag cluster ensembles [42]. The resonance is interpreted as an oscillation of the free silver electron-gas perpendicular to the substrate plane. The corresponding in plane oscillation (1,1)-mode) is not accessible to the experiment because the incoming electrons from the tip induce preferentially a dipole or impact excitation along the surface normal. Additionally, the (1,1)-mode is strongly damped by its image dipole induced in the NiAl substrate. For a detailed discussion see ref. [41].

The energy position and the line width of the Mie plasmon show a characteristic dependence on cluster size [41] (see Fig. 11). For decreasing cluster diameter from 12.0 to 1.5 nm a blue shift of the plasmon energy from 3.6 eV to almost 4.0 eV is observed. In the same size range the homogeneous line width of the emission increases from

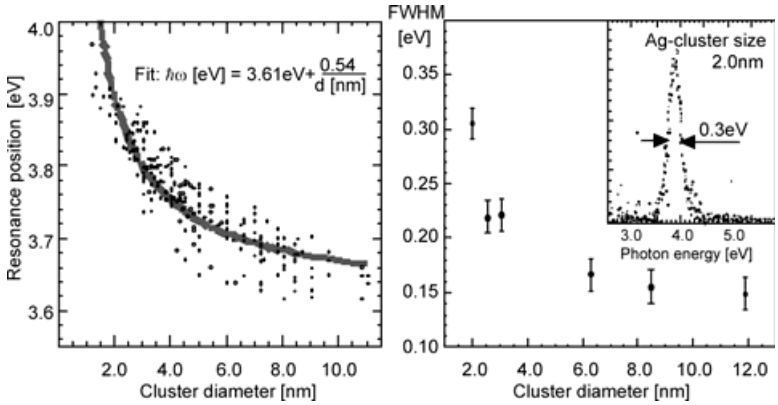

Fig. 11. Energetic position and line width of the Mie resonance as a function of cluster diameter

160 meV to 300 meV. Both size dependencies show an $1/d$ (d = cluster diameter) behavior reflecting the growing surface contribution with respect to bulk effects in small particles. For the blue shift of the peak position changes of the intrinsic electronic properties in a spatially confined system are considered. In the case of Ag particles the plasmon energy is determined by the classical Drude frequency of the free 5s electrons drastically reduced by a strong screening effect of the 4d electrons [44]. The 4d depolarization field vanishes at the cluster surface because the 4d electrons are more localized at the Ag atoms and have a low residence probability outside the classical cluster volume. In contrast, a fraction of the Ag 5s electrons spills out into the vacuum, where they are unaffected by the 4d screening and increase their plasmon frequency. With decreasing cluster size this fraction of free electrons residing outside the classical cluster volume increases with respect to the total electron number and the Mie plasmon energy shifts to higher energies. This effect is partly cancelled, because a considerable electron spill out results also in a reduction of the electron density inside the cluster volume and thus a red shift of the plasmon energy with decreasing cluster size ($\omega^2_{\text{plasmon}} \sim n_{\text{electron}}$). However, in the present experiment the electron spill out is strongly quenched at the cluster–alumina interface and the blue shift dominates the size dependence of the Mie plasmon. A quantitative description of the experimental results has to treat the 5s–4d interaction on a fully quantum-mechanical level and has to include the restructuring of the bulk electronic structure in small Ag particles.

For the increase of the homogeneous line width of the Mie resonance with decreasing cluster size, only an empirical model can be presented as well. The behavior reflects the reduced lifetime of the collective electron oscillation in small particles due to an enhanced electron–surface scattering rate. This additional decay mechanism (apart from electron–electron, electron–phonon scattering and Landau damping) becomes highly efficient, when the electron mean free path exceeds the cluster diameter and causes a dephasing process of the collective oscillation [42]. The surface mediated character of the damping with respect to the cluster volume can explain the observed 1/d behavior of the line width with decreasing cluster size.

4. Magnetic Properties of Deposited Metal Aggregates

In addition to investigations on electronic properties it is interesting to develop tools which allow us to study magnetic properties. Based upon the experience using electron spin resonance (ESR) on radicals adsorbed on single crystal surfaces [45–47] we have started measurements of the ferromagnetic resonance (FMR) [48, 49] of deposited aggregates. To this end we prepare either a bulk single crystal oxide surface or an epitaxial thin oxide film under ultrahigh vacuum conditions and grow the metal aggregates on it. Such a sample is brought into a microwave cavity and the FMR is recorded. The sample, which is attached to a manipulator may be oriented with respect to the external field, and therefore the orientation of the direction of the magnetization is accessible.

Figure 12a shows such a measurement for Co particles on $Al_2O_3(0001)$, deposited at room temperature. An uniaxial orientation is found with a single minimum at orientation of the field parallel to the surface plane. This means that the magnetization is also oriented in this way [49]. A very similar behavior is found for iron as plotted in

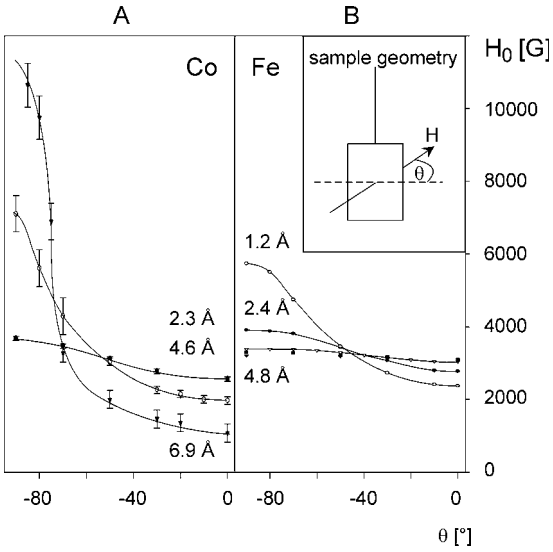

Fig. 12. Angular dependence of the resonance field for various amounts of Co (part A) and Fe (part B) deposited at room temperature on an $Al_2O_3(0001)$ single crystal surface. θ denotes the angle between the ctystal surface and the static magnetic field. The deposited amounts are given in terms of the effective layer thickness

Fig. 12b. The smaller asymmetry is a property of the specific metal. While upon heating the behavior does not change for Co, it becomes more complex for Fe (see Fig. 13) [50].

This is indicative for the survival of uniaxial magnetism in the hexagonal cobalt and its breakdown for the body centered cubic iron. Fe(bcc) has three easy axes of magnetization and the formation of more crystalline aggregates is likely to be the reason for the observation.

Since atomic resolution is very hard to achieve on the small aggregate at present, these experimental observations in the ferromagnetic resonance are very useful. FMR can also be used to follow adsorption on the aggregates. We find that chemisorption of CO quenches the surface magnetism of the small particles. Oxidation of the small parti-

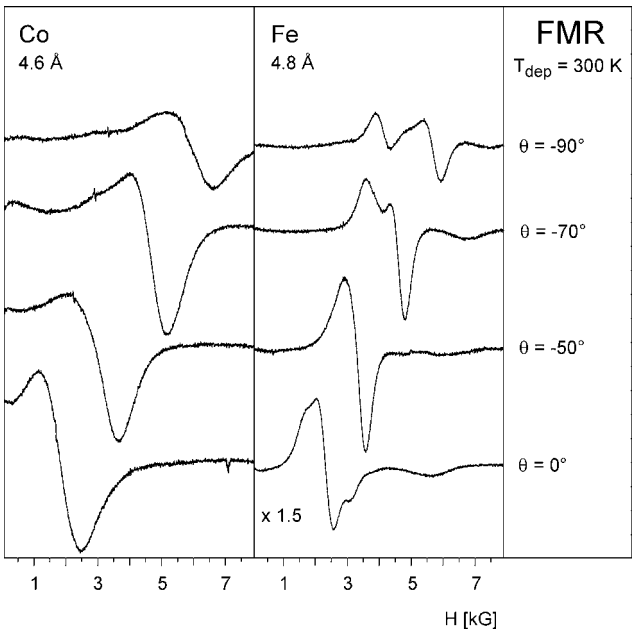

Fig. 13. Comparison of the angular dependent FMR spectra of Co and Fe on $Al_2O_3(0001)$ after heating the deposits (prepared at 300 K) to 870 K. The spectra were recorded at 300 K. θ denotes the angle between the static magnetic field and the crystal surface. The deposited amounts are given in terms of the effective layer thickness

cles leads to the formation of an oxide skin on a ferromagnetic kernel. Since the oxide signal occurs at very different fields only the FMR of the kernel has been recorded. Such measurements may be used to follow the formation of oxide aggregates deposited on oxide supports which would have interesting catalytic properties.

5. Adsorption at Ambient Conditions

It is the next step to investigate adsorption and reaction of molecules on the surfaces of the deposited metal aggregates. Several groups have used Fourier Transform Infrared (FTIR) spectroscopy to study adsorption on such systems [51]. The results have been published and discussed in several review articles [4, 51].

It is quite reasonable to consider that adsorbed gases could influence the structure of deposited clusters even under UHV conditions. However, at elevated pressures the effect may be more pronounced. But even if the aggregate surfaces remained unaffected and behave rigid, the structure of an adsorbate under reaction conditions is probably still different from that in UHV experiments.

At the high pressure of a catalytic reaction surface coverages may be obtained that can not be reproduced by the small exposures of surface science studies (typically on the order of Langmuirs, 10^{-6} Torr sec). If the "saturation" coverage of UHV experiments is exceeded, new adsorbate structures may form, as shown e.g. by a high pressure STM study of CO on Pt(111) [52]. Furthermore, at high pressure weakly adsorbed species are present with much higher concentration (resulting from a higher rate of adsorption) than under low pressure when they quickly desorb [53]. In the most unfavorable case, prominent species of low pressure studies may simply be spectators under high pressure conditions.

In order to tackle this problem a surface sensitive technique is needed that allows to monitor adsorbates under reaction conditions ($\sim$1 bar). A high pressure environment prevents the use of electron spectroscopies but is compatible with photon-based techniques such as infrared-visible sum frequency generation (SFG) spectroscopy. IR-vis SFG is a type of laser spectroscopy that is able to acquire vibrational spectra of adsorbates from UHV to ambient conditions. Due to its inherent surface sensitivity, surface vibrational spectra can be recorded even in the presence of a gas phase, in contrast to infrared reflection absorption spectroscopy (IRAS) that encounters problems with the excitation of rotational bands in the gas phase at pressures >1 mbar, obstructing the surface species information. A detailed description of the SFG process can be found in the literature [53–56]. SFG is a second-order nonlinear optical process which involves the mixing of tunable infrared (ω_{IR}) and visible light (ω_{vis}) to produce a sum frequency output ($\omega_{SFG} = \omega_{IR} + \omega_{vis}$). The process is only allowed in a medium without inversion symmetry (in the electric dipole approximation), e.g. at surfaces where the inversion symmetry is broken. The dominant SFG signal is hence generated by the modes of the adsorbate, while the centrosymmetric bulk of face-centered cubic metals and an isotropic gas phase give nearly zero contribution to the SFG signal.

It has been frequently discussed [1–10] that single crystals can not fully represent supported metals. In order to include size and electronic effects, surface rearrangements, etc. in a pressure-dependent study of gas adsorption SFG spectroscopy should be ideally carried out on supported nanoparticles. Although the applicability of SFG spectroscopy to nano-structured supported catalysts has been questioned for several

reasons (scattering of laser beams on rough surfaces, disordered adsorbates, small total coverages), we recently succeeded to obtain SFG spectra from CO adsorbed on supported Pd nanoclusters [57]. $Pd/Al_2O_3/NiAl(110)$ model catalysts were prepared as described above, and transferred under vacuum to a SFG-compatible UHV compatible high pressure cell. Details about the sample preparation and cell design are published elsewhere [54, 57].

Figure 14 shows SFG spectra of CO adsorption on alumina supported Pd particles of 3 nm mean size (about 300 atoms per particle), grown at 90 K (particle density 10^{13} cm^2). According to LEED and STM measurements [4, 58], the particle surface exhibits a high defect density as a result of the low growth temperature. Figure 14a displays SFG spectra taken at 190 K. Two peaks are clearly identified at 10^{-7} mbar CO and, according to IRAS results on Pd single crystals [59–61], they originate from bridge bonded CO at 1976 cm^{-1} and from terminal (on-top) CO at 2106 cm^{-1}. If one takes the integrated SFG signal intensity as a measure of the ratio of on-top to bridge-bonded CO, a value of about 0.5 is obtained. However, this value is only taken as an estimate here, since the SFG intensity can not be easily correlated with the concentration of a particular surface species. The coexistence of bridge and on-top bonded CO, a situation which is not found on Pd single crystals, reflects the defective structure of the Pd nanoparticles. In fact, the site occupancy on the Pd aggregates compares best with defect-rich single crystal Pd(111) or rough Pd thin films [59, 60, 62]. The difference between supported Pd aggregates and Pd(111) could result from a reduced lateral CO interaction on the nanoparticles or from the presence of additional crystal planes.

Increasing the pressure to 1, 10 and 200 mbar CO had only a small effect on the peak frequencies and also the ratio of on-top vs. bridge-bonded CO was nearly unchanged (Fig. 14a). If the sample temperature is raised to 300 K (Fig. 14b), which is above the desorption temperature of on-top CO on Pd clusters under UHV conditions [4], bridge-bonded CO is the only species that can be observed by SFG at 10^{-7} mbar. However, the on-top adsorption sites can be populated at $p \geq 1$ mbar, and at 200 mbar CO a relative on-top/bridge ratio of ~ 0.5 can be obtained, similar to the value at 190 K.

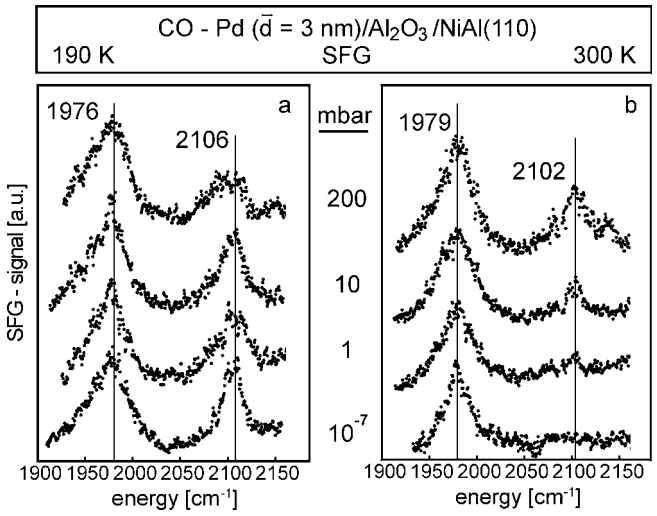

Fig. 14. SFG spectra of CO adsorption on a $Pd/Al_2O_3/NiAl(110)$ model catalyst at a) 190 and b) 300 K (3 nm Pd particles grown at 90 K). The observed resonances are characteristic of bridge-bonded CO and terminally-bonded CO can be re-populated at $\geq$1 mbar

Comparing Figs. 14a and b illustrates the pressure- and temperature-dependent adsorption site occupancy of CO on Pd/Al_2O_3. While at 190 K an extrapolation of the 10^{-7} mbar spectrum to 200 mbar would lead to a satisfactory result, for a temperature of 300 K the prediction would be wrong (absence vs. presence of on-top CO). In addition, the adsorption site occupancy of Pd nanoparticles is influenced by the particle size and surface structure. If the same experiment is carried out on Pd particles grown at 300 K that mainly exhibit well-developed (111) surface facets, the adsorption behavior is again different [57]. These measurements could be repeated several times indicating that significant structural changes of the particles were absent - which seems reasonable at the low temperatures applied. Our adsorption study clearly demonstrates the need to characterize adsorbates under reaction conditions. If this is carried out under several bars of pressure and at higher temperature even more pronounced effects are expected. This represents an important field of research in the immediate future.

6. Synopsis

The present review highlighted some recent experiments performed on metal aggregates deposited on an oxide substrate representing model systems for heterogeneous catalysts. Insight into the structure of individual aggregates may be gained. Experiments are underway to unravel the elementary stages in cluster formation, i.e. diffusion of metal atoms on oxide surfaces. Two areas have been addressed which need further attention in future studies: One concerns the investigation of the magnetic properties of deposited aggregates, the other one deals with the influence of ambient conditions on adsorption as well as structure of systems. We demonstrate that there are methods available that allow us to study many aspects of such model systems. Surface science is moving into a direction to start to close both the materials as well as the pressure gaps towards catalysis.

References

[1] G. ERTL and H.-J. FREUND, Physics Today **52**, 32 (1999).
[2] H.-J. FREUND, M. BÄUMER, and H. KUHLENBECK, Adv. Catal. **45**, 333 (2000).
[3] H.-J. FREUND, Ber. Bunsenges. Phys. Chem. **99**, 1261 (1995).
[4] M. BÄUMER and H.-J. FREUND, Progr. Surf. Sci. **61**, 127 (1999).
[5] D. W. GOODMAN, Surf. Rev. Lett. **2**, 9 (1995).
[6] P. L. J. GUNTER, J. W. H. NIEMANTSVERDRIET, F. H. RIBEIRO, and G. A. SOMORJAI, Catal. Rev. Sci. Eng. **39**, 77 (1997).
[7] D. A. BONNELL, Progr. Surf. Sci. **57**, 187 (1998).
[8] C. B. DUKE (Ed.), Surface Science: The First Thirty Years (Elsevier, Amsterdam), **299/300**, (1994).
[9] H. POPPA, Catal. Rev. Sci. Eng. **35**, 359 (1993).
[10] C. R. HENRY, Surf. Sci. Rep. **31**, 231 (1998).
[11] M.-C. WU and P. J. MØLLER, Surf. Sci. **224**, 250 (1989).
[12] P. J. MØLLER and M.-C. WU, Surf. Sci. **224**, 265 (1989).
[13] M. C. WU and P. J. MØLLER, Surf. Sci. **235**, 228 (1990).
[14] P. J. MØLLER and J. NERLOV, Surf. Sci. **307–309**, 591 (1993).
[15] U. DIEBOLD, J.-M. PAN, and T. E. MADEY, Surf. Sci. **331–333**, 845 (1995).
[16] P. W. MURRAY, J. SHEN, N. G. CONDON, S. J. PANG, and G. THORNTON, Surf. Sci. **380**, L455 (1997).
[17] P. STONE, R. A. BENNETT, and M. BOWKER, New J. Phys. **1**, 8 (1998-1999).
[18] O. DULUB, W. HEBENSTREIT, and U. DIEBOLD, Phys. Rev. Lett. **84**, 3646 (2000).

[19] T. Schröder, M. Adelt, B. Richter, M. Naschitzki, M. Bäumer, and H.-J. Freund, Surf. Rev. Lett. **7**, 7 (2000).
[20] F. J. Grunthaner, P. J. Grunthaner, R. P. Vasquez, B. F. Lewis, J. Maserjian, and A. Madhukar, J. Vac. Sci. Technol. **16**, 1443 (1979).
[21] J. Libuda, F. Winkelmann, M. Bäumer, H.-J. Freund, T. Bertrams, H. Neddermeyer, and K. Müller, Surf. Sci. **318**, 61 (1994).
[22] R. M. Jaeger, H. Kuhlenbeck, H.-J. Freund, M. Wuttig, W. Hoffmann, R. Franchy, and H. Ibach, Surf. Sci. **259**, 235 (1991).
[23] J. Libuda, M. Frank, A. Sandell, S. Andersson, P. A. Brühwiler, M. Bäumer, N. Mårtensson, and H.-J. Freund, Surf. Sci. **384**, 106 (1997).
[24] S. Stempel, M. Bäumer, and H.-J. Freund, Surf. Sci. **402–404**, 424 (1998).
[25] M. Heemeier, PhD-Thesis, Freie Universität Berlin, (in preparation).
[26] A. Piednoir, E. Perrot, S. Granjeaud, A. Humbert, C. Chapon, and C. R. Henry, Surf. Sci. **391**, 19 (1997).
[27] K. H. Hansen, T. Worren, S. Stempel, E. Lægsgaard, M. Bäumer, H.-J. Freund, F. Besenbacher, and I. Stensgaard, Phys. Rev. Lett. **83**, 4120 (1999).
[28] M. Methfessel, D. Hennig, and M. Scheffler, Phys. Rev. B **46**, 4816 (1992).
[29] A. Bogicevic and D. R. Jennison, Phys. Rev. Lett. **82**, 4050 (1999).
[30] M. Klimenkov, S. Nepijko, H. Kuhlenbeck, M. Bäumer, R. Schlögl, and H.-J. Freund, Surf. Sci. **391**, 27 (1997).
[31] N. Ernst, B. Duncombe, G. Bozdech, M. Naschitzki, and H.-J. Freund, Ultramicroscopy **79**, 231 (1999).
[32] N. Nilius, A. Cörper, G. Bozdech, N. Ernst, and H.-J. Freund, Progr. Surf. Sci., (in press).
[33] G. L. Kellogg, Surf. Sci. Rep. **21**, 1 (1994).
[34] A. Cörper, G. Bozdech, N. Ernst, and H.-J. Freund, personal communication
[35] A. Sandell, J. Libuda, P. A. Brühwiler, S. Andersson, M. Bäumer, A. J. Maxwell, N. Mårtensson, and H.-J. Freund, Phys. Rev. B **55**, 7233 (1997).
[36] A. Bettac, L. Köller, V. Rank, and K. H. Meiwes-Broer, Surf. Sci. **402**, 475 (1998).
[37] M. Valden, X. Lai, and D. W. Goodman, Science **281**, 1647 (1998).
[38] B. C. Stipe, M. A. Rezaei, and W. Ho, Science **280**, 1732 (1998).
[39] J. H. Coombs, J. K. Gimzewski, B. Reihl, J. K. Sass, and R. R. Schlittler, J. Microscopy **152**, (1988).
[40] R. Berndt, in Scanning Probe Microscopy, edited by R. Wiesendanger (Springer, Berlin, 1998), p. 97.
[41] N. Nilius, N. Ernst, and H.-J. Freund, Phys. Rev. Lett. **84**, 3994 (2000).
[42] U. Kreibig and M. Vollmer (Ed.), Optical Properties of Metal Clusters (Springer, Berlin), **25**, (1995).
[43] N. Nilius, N. Ernst, H.-J. Freund, and P. Johansson, Phys. Rev. B **61**, 12682 (2000).
[44] A. Liebsch, Phys. Rev. B **48**, 11317 (1993).
[45] H. Schlienz, M. Beckendorf, U. J. Katter, T. Risse, and H.-J. Freund, Phys. Rev. Lett. **74**, 761 (1995).
[46] U. J. Katter, T. Hill, T. Risse, H. Schlienz, M. Beckendorf, T. Klüner, H. Hamann, and H.-J. Freund, J. Phys. Chem. B **101**, 552 (1997).
[47] T. Risse, T. Hill, J. Schmidt, G. Abend, H. Hamann, and H.-J. Freund, J. Chem. Phys. **108**, 8615 (1998).
[48] T. Hill, M. Mozaffari-Afshar, J. Schmidt, T. Risse, S. Stempel, M. Heemeier, and H.-J. Freund, Chem. Phys. Lett. **292**, 524 (1998).
[49] T. Hill, S. Stempel, T. Risse, M. Baeumer, and H.-J. Freund, J. Magn. Mag. Mater. **198–199**, 354 (1999).
[50] T. Hill, PhD-Thesis, Ruhr-Universität Bochum, (1998).
[51] D. R. Rainer and D. W. Goodman, in Chemisorption and Reactivity on Supported Clusters and Thin Films, edited by R. M. Lambert and G. Pacchioni (Kluwer, Dordrecht, 1997), Vol. 331, (p. 27).
[52] J. A. Jensen, K. B. Rider, M. Salmeron, and G. A. Somorjai, Phys. Rev. Lett. **80**, 1228 (1998).
[53] G. A. Somorjai and G. Rupprechter, J. Phys. Chem. B **103**, 1623 (1999).
[54] G. Rupprechter, T. Dellwig, H. Unterhalt, and H.-J. Freund, Topics in Catalysis, (in press (2001)).

[55] Y. R. Shen, Surf. Sci. **299/300**, 551 (1994).
[56] J. Miragliotta, P. Rabinowitz, S. D. Cameron, and R. B. Hall, Appl. Phys. A **51**, 221 (1990).
[57] T. Dellwig, G. Rupprechter, H. Unterhalt, and H.-J. Freund, Phys. Rev. Lett. **85**, 776 (2000).
[58] M. Bäumer, J. Libuda, A. Sandell, H.-J. Freund, G. Graw, T. Bertrams, and H. Neddermeyer, Ber. Bunsenges. Phys. Chem. **99**, 1381 (1995).
[59] F. M. Hoffmann, Surf. Sci. Rep. **3**, 103 (1983).
[60] M. Tüshaus, W. Berndt, H. Conrad, A. M. Bradshaw, and B. Persson, Appl. Phys. A **51**, 91 (1990).
[61] W. K. Kuhn, J. Szanyi, and D. W. Goodman, Surf. Sci. Lett. **274**, L611 (1992).
[62] A. M. Bradshaw and F. M. Hoffmann, Surf. Sci. **52**, 449 (1975).